Airfoil data sensitivity analysis for actuator disc simulations used in wind turbine applications

Nilsson, Karl; Breton, Simon-Philippe; Sørensen, Jens Nørkær; Ivanell, Stefan

Published in:
Journal of Physics: Conference Series (Online)

Link to article, DOI:
10.1088/1742-6596/524/1/012135

Publication date:
2014

Document Version
Publisher's PDF, also known as Version of record

Airfoil data sensitivity analysis for actuator disc simulations used in wind turbine applications

2014 J. Phys.: Conf. Ser. 524 012135

(http://iopscience.iop.org/1742-6596/524/1/012135)

Airfoil data sensitivity analysis for actuator disc simulations used in wind turbine applications

Karl Nilsson[1,2], Simon-Philippe Breton[1], Jens N. Sørensen[3] and Stefan Ivanell[1,2]

[1]Department of Earth Sciences, Wind Energy section, Uppsala University Campus Gotland, Cramérgatan 3, 621 57, Visby, Sweden
[2]Linné Flow Centre, Department of Mechanics, KTH, Stockholm, Sweden
[3]DTU Wind Energy, DTU, Kgs. Lyngby, Denmark

E-mail: karl.nilsson@geo.uu.se

Abstract. To analyse the sensitivity of blade geometry and airfoil characteristics on the prediction of performance characteristics of wind farms, large-eddy simulations using an actuator disc (ACD) method are performed for three different blade/airfoil configurations. The aim of the study is to determine how the mean characteristics of wake flow, mean power production and thrust depend on the choice of airfoil data and blade geometry. In order to simulate realistic conditions, pre-generated turbulence and wind shear are imposed in the computational domain. Using three different turbulence intensities and varying the spacing between the turbines, the flow around 4-8 aligned turbines is simulated. The analysis is based on normalized mean streamwise velocity, turbulence intensity, relative mean power production and thrust. From the computations it can be concluded that the actual airfoil characteristics and blade geometry only are of importance at very low inflow turbulence. At realistic turbulence conditions for an atmospheric boundary layer the specific blade characteristics play an minor role on power performance and the resulting wake characteristics. The results therefore give a hint that the choice of airfoil data in ACD simulations is not crucial if the intention of the simulations is to compute mean wake characteristics using a turbulent inflow.

Nomenclature

c	Local chord of the blade	$\overline{T}_{rel}$	Relative mean thrust $\frac{\overline{T}}{\overline{T}_1}$
f_z	Normal force per unit area	TI_{amb}	Ambient turbulence intensity (0%, 4.5%, 8.9%)
f_θ	Tangential force per unit area	TI_{WT}	Turbulence intensity in wake $\frac{\sigma_z}{U_0}$
r	Local radius	U_0	Free stream velocity (8 m/s)
z, x, y	Streamwise, crosswise and vertical coordinates	$\overline{W}$	Mean streamwise velocity
A	Disc area	$\overline{W}_{norm}$	Normalized mean streamwise velocity $\frac{\overline{W}}{U_0}$
P	Power	λ	Tip speed ratio
$\overline{P}$	Mean power	σ_i	Standard deviation of velocity components
$\overline{P}_1$	Mean power of the first turbine in the row	Δt	Time step used in LES ($0.025R/U_0$)
$\overline{P}_{rel}$	Relative mean power $\frac{\overline{P}}{\overline{P}_1}$	Δt_{Mann}	Time step of Mann box ($0.16R/U_0$)
R	Rotor radius (46.5 m)	Δx	Equidistant resolution of the grid ($0.1R$, $0.05R$)
T	Thrust	Φ	Local twist of the blade
$\overline{T}$	Mean thrust	Ω	Anglular velocity
$\overline{T}_1$	Thrust of first turbine in the row		

1. Introduction

The actuator disc (ACD) method (Sørensen and Myken [1]) has been largely exploited in the last two decades and has proven to be a reliable tool for wind farm power predictions in combination with large-eddy simulations (see e.g. Nilsson *et al.* [2]).

Later contributions in the field using LES are due to, among others, Ivanell *et al.* [3], Porté-Agel *et al.* [4], Troldborg *et al.* [5][6], Churchfield *et al.* [7], Keck *et al.* [8] and Troldborg *et al.* [9]. In the work by Ivanell *et al.* [3] a farm consisting of nine turbines was studied, and special interest was placed on the dependency on the inflow angle of the wind and the impact of considering a turbulent inflow. Porté-Agel *et al.* [4] studied the velocity and the turbulent statistics after a single turbine using an ACD method with constant loading (this method is referred to as ACD-NR), an ACD method which uses airfoil data and considers turbine-induced flow rotation (ACD) and an actuator line (ACL) method. The results were compared with wind tunnel measurements and demonstrated that the ACD and ACL methods gave very similar results that were in good agreement with measured data whereas the results of the ACD-NR deviated significantly from the measurements. Troldborg *et al.* [5][6] performed LES computations using an ACL method on a single turbine in uniform inflow conditions and on two turbines where the inlet flow was varied to mimic laminar, offshore and onshore conditions. Churchfield *et al.* [7] performed computations on two aligned turbines using flexible ACLs to model the rotor blades. The turbines were placed in a turbulent atmospheric boundary layer, and the aim of the work was to study the effect of varying the surface roughness and atmospheric stability on power production, structural loads and wake evolution. Keck *et al.* [8] described and verified a method to introduce a prescribed wind shear in combination with pre-generated synthetic turbulence. Troldborg *et al.* [9] performed further verifications of the prescribed wind shear and the pre-generated synthetic turbulence described in Keck *et al.* [8] using a simple linear shear approach. For an extensive list of different wake models, it is referred to Crespo *et al.* [10] and Vermeer *et al.* [11].

For validation purposes, the results from simulations are often compared to production data from real wind farms. Airfoil data and blade geometry for real turbines are in many cases not publicly available. Therefore, in simulations these are often based on alternative synthetic data, as the NREL 5MW turbine (Jonkman *et al.* [12]) which are scaled to fit the real turbines. The aim of this work is to investigate the influence on the wake conditions when using different rotors and determine the importance of the airfoil data when analyzing mean wake flow characteristics. In the present work three different sets of airfoil data (described in Section 2) are used to simulate a row of wind turbines. These airfoils are imposed in three flow conditions (described in Section 7) characterized by ambient turbulence intensities (TI_{amb}) equal to 0%, 4.5% and 8.9%, respectively. Furthermore, the spacing between the turbines is varied between $6.6R$ and $14R$. These spacings are chosen by looking at the Horns Rev wind farm at an inflow angle of 270° and at the Lillgrund wind farm at an inflow angle of 120°, corresponding to a spacing of $14R$ and $6.6R$, respectively.

The wake flow is analyzed in terms of normalized mean streamwise velocity ($\overline{W}_{norm}$) and turbulence intensity (TI_{WT}). Additionally, the relative mean power production ($\overline{P}_{rel}$) and thrust ($\overline{T}_{rel}$) of the individual turbines are investigated.

2. Turbine specifications and positioning

In this study data sets from three different airfoils are used, which all are representations of the Siemens SWT-2.3-93 turbine used in e.g. the Lillgrund wind farm. The first turbine is a downscaled NREL turbine (Jonkman *et al.* [12]) with a nominal power of 2.3 MW. This downscaled turbine is described in detail in Nilsson *et al.* [2] and is in this study referred to as AF1. The second turbine is based on the DU21 profile which is one of the profiles used in the AF1 turbine. This profile is used for the entire span width of the rotor. The chord (c) and twist

(Φ) distributions are designed to fit the C_P and C_T curves of AF1. This turbine is referred to as AF2. The third turbine is the generic SWT-2.3-93 turbine which is described in detail in Churchfield [13]. This turbine is in the current study referred to as AF3. The twist and chord distributions for the different airfoils are depicted in Figure 1.

In this study all turbines are set to operate at a fixed rotational velocity determined by a tip speed ratio (λ) equal to 8.5 based on the free stream velocity (U_0). The first turbine is in all cases imposed at z =17R, where R is the rotor radius ($R = 46.5$m). Due to grid size limitations, 4 turbines are used in the $14R$ spacing case while 8 are used in the $6.6R$ case.

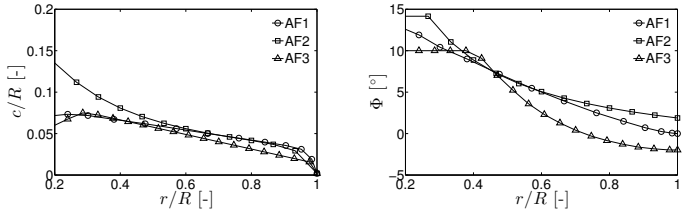

Figure 1. Chord (left) and twist (right) distributions of the three rotor configurations.

3. Numerical model

In this study the EllipSys3D code (Michelsen [14][15] and Sørensen [16]) is used. The EllipSys3D code is a general purpose Navier-Stokes solver which solves for incompressible flows using a finite volume approach. The code is well documented and will not be described in detail here. Briefly, the computations are performed using the LES technique where large eddies are resolved explicitly and eddies smaller than a certain size are filtered out and modeled by an eddy-viscosity based sub-grid scale (SGS) model. For this work the mixed scale model developed by Ta Phuoc [19] is used. It is referred to Mikkelsen [17], Ivanell *et al.* [18], Troldborg *et al.* [5] and Nilsson *et al.* [2] among others for more information about the numerical model.

4. Computational domain and boundary conditions

In the current study, a computational domain measuring $80\times20\times20R^3$ is used. The center part of the domain is equidistant, with a spacing equal to Δx, and this region measures $60\times4\times4R^3$. The parts outside the equidistant region are stretched towards the outer boundaries. A schematic drawing of the domain is shown in the left part of Figure 2. Dirichlet conditions are imposed at the inlet for pressure and velocities, a convective condition is imposed at the outlet, periodical conditions are imposed at the sides and slip conditions are imposed at the top and the bottom of the domain.

The computational time step (Δt) is chosen conservatively to $0.025R/U_0$ in order not to violate the Courant-Friedrichs-Lewy (CFL) condition.

Δx is chosen to $0.1R$ based on experiences from earlier simulations. However, to show the behavior of using a more refined model some simulations are performed with $\Delta x = 0.05R$. This grid resolution could not be used for all simulations due to limitations in computational capability.

5. Actuator disc method

The turbines are in this study represented using actuator discs (ACD). The rotor is implemented in the simulation using a body force approach. This method significantly reduces the computational demands compared to modeling the full geometry of the rotor since the boundary layer over the blades is not resolved. However, as this method makes use of airfoil data (C_L and

C_D distributions as functions of the angle of attack) the results depend on the quality of these data. This dependency is the subject of investigation in this study. The ACD method used is described in Nilsson *et al.* [2]. For this study the ACD is discretized using 21 points along the rotor radius and 81 points in the azimuthal direction. In order to avoid numerical problems, the body forces are smeared in a Gaussian manner in the streamwise direction using a standard deviation of $0.2R/\sqrt{2}$.

6. Collecting and analyzing data

The simulations are performed with 80,000 time steps each. The last 41,300 time steps are used in the analysis corresponding to 100 minutes of physical time to ensure having a quasi-stationary solution.

In order to store the outcome of the simulations, time series of velocity, probe sheets are inserted in the domain at positions $(z, 10, 10)$. In the cases without wind turbines the sheets are inserted at z positions starting at $17R$, followed by $24R$ and then with a spacing of $14R$. The conditions at $17R$ are used for determination of TI_{amb}. In the cases with turbines, z are the positions in the middle of each pair of turbines. Additionally, in order to have a detailed description of the flow upstream and downstream of the first turbine, sheets are inserted using a spacing of $1R$ in this region. For a turbine spacing of $6.6R$ this region is defined by $13R \leq z \leq 23R$ while for a turbine spacing of $14R$ it is defined as $13R \leq z \leq 31R$. The sheets consist of a number of circles and on these circles a number of points are assigned in the azimuthal direction. In the present study 15 circles are used (including the center point), which are separated with a distance of Δx, and 4 points are used in the azimuthal direction, as depicted in the right part of Figure 2. Totally 59 points are evaluated and on each of these, the streamwise, crosswise and vertical velocity components are saved at each time step.

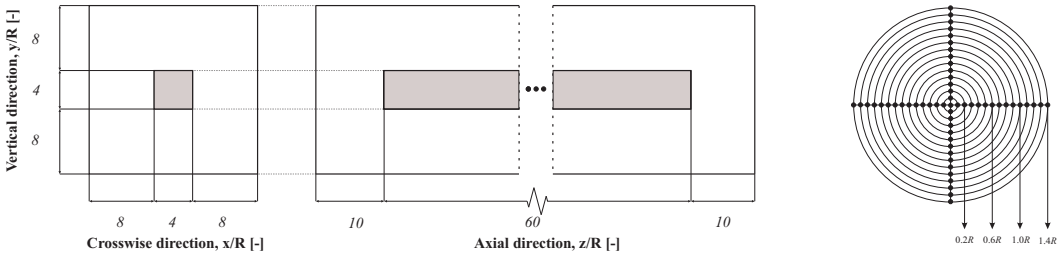

Figure 2. A sketch of the grid structure (left) and a schematical figure explaining the probe sheet used for collection of velocity time series (right).

For the determination of the conditions in the flow domain in absence of turbines, standard deviations for all components (σ_i) are analyzed. For the cases in the presence of turbines only the streamwise component is analyzed in terms of normalized mean velocity ($\overline{W}_{norm}$) and turbulence intensity (TI_{WT}). TI_{WT} is defined as the streamwise standard deviation (σ_z) normalized by U_0. It is noted here that the mean value of the 59 points on the probe sheet is considered in the calculations.

The power (P) and thrust (T) are saved for each turbine (ACD) at each time step and are computed employing the following equations,

$$P = \Omega \int \int_A f_\theta r dA, \; T = \int \int_A f_z dA \tag{1}$$

where Ω is the angular velocity, A is the disc area, f_θ is the tangential force and f_z is the normal force per unit area on the disc. In the analysis the relative mean values of power ($\overline{P}_{rel}$) and thrust ($\overline{T}_{rel}$) are evaluated.

7. Shear and atmospheric turbulence

The simulations are performed with an ambient turbulence intensity (TI_{amb}) equal to 0%, 4.5% and 8.9%. The atmospheric turbulence is pre-generated using the method of Mann (Mann [20][21]). In this method, isotropic von Kármán turbulence is exposed to a linear shear using rapid distortion theory. The result is an anisotropic turbulence which, in our case, is fitted to the Kaimal spectrum. In the used application of the method of Mann the user sets a height, a mean velocity and a roughness length as inputs. In the current cases, the height is set to 68 m, the mean velocity to 8 m/s and the roughness lengths to $2.0 \cdot 10^{-5}$ m and $3.5 \cdot 10^{-2}$ m for TI_{amb} equal to 4.5% and 8.9%, respectively. The linear shear profile used in the Mann algorithm has a shear exponent equal to 0.0923 s^{-1} and 0.1338 s^{-1} for TI_{amb} equal to 4.5% and 8.9%, respectively. The results from the method of Mann is a box of turbulence. This box measures $333 \times 3.9 \times 3.9R^3$ with an equidistant resolution of approximately ($0.16R$, $0.12R$, $0.12R$) in (z, x, y) directions. The box consists of 2048×32×32 grid points. Each position in the z direction is, using Taylor's frozen hypothesis, a time step. The time step of the Mann box (Δt_{Mann}) is therefore approximately equal to $0.16R/U_0$. In the simulations, xy planes of turbulence are imposed, using body forces, at a certain z position at a rate determined by Δt_{Mann} and Δt. These planes are then being convected downstream by the flow solver. As the spatial and temporal resolution of the Mann box is lower than in the grid in the simulations, interpolation is required. In the present study, the turbulence planes are imposed at $z = 13R$ as depicted in the left part of Figure 3. As previously stated, the results are based of 100 minutes of simulation data. Within this time period the Mann box is repeated approximately 3 times, which imposes artificial periodicity in the results. However, as all rotor configurations are exposed to this periodicity, the effects of this are believed to the marginal.

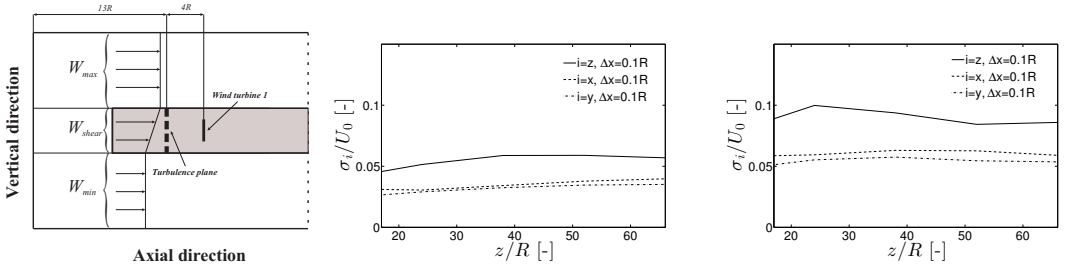

Figure 3. Linear shear profile and turbulence plane position (left), normalized standard deviations for TI_{amb}=4.5% (middle) and TI_{amb}=8.9% (right) in absence of turbines.

A prescribed wind shear is imposed, also depicted in the left part of Figure 3, using an analogy to the immersed boundary layer using body forces. In this study a simplified linear shear is used as suggested by Troldborg *et al.* [9]. The prescribed linear shear profile is identical to that used in the method of Mann. The normalized standard deviation components as function of the downstream distance, in the absence of wind turbines, are depicted in the middle and right parts of Figure 3, and it can be seen that the turbulence remains reasonably close to the imposed conditions throughout the domain. This is analogous to what was observed and discussed in Troldborg *et al.* [9].

8. Results and discussion

8.1. Relative mean power

The relative mean power ($\overline{P}_{rel}$) is in Figures 4 and 5 depicted as function of downstream distance for turbine spacings of $6.6R$ and $14R$, respectively. In the figures, measurement data for the Lillgrund and the Horns Rev wind farms have been added for comparison purposes. The

Lillgrund (LG) data (Nilsson *et al.* [2]) is based on a turbine spacing of $6.6R$ and a TI_{amb} equal to approximately 5%. The Horns Rev (HR) data (Hansen [22]) is based on a turbine spacing of $14R$ and a TI_{amb} equal to approximately 7% (Hansen *et al.* [23]). Furthermore, due to the shape of the farm layouts, the LG data is based on a single row of turbines (Row D in Nilsson *et al.* [2]) while the HR data is based on averaging of all rows in the farm. Since the simulations are not exact representations of the measurement cases (e.g. in terms of TI_{amb} and farm layouts), the comparisons are limited. However, it is emphasized that the actual comparison in this study is between different rotor configurations and that the measurement data only is used to show that the production levels in the simulations are at an adequate level.

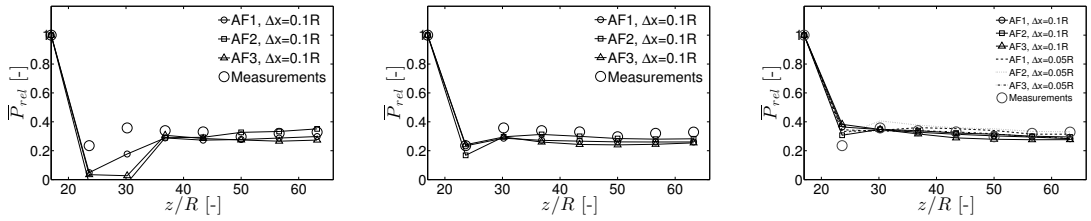

Figure 4. Relative mean power for TI_{amb}=0% (left), TI_{amb}=4.5% (middle) and TI_{amb}=8.9% (right) in the presence of wind turbines with a spacing of $6.6R$. TI_{amb} in the measurement case is always equal to 5%.

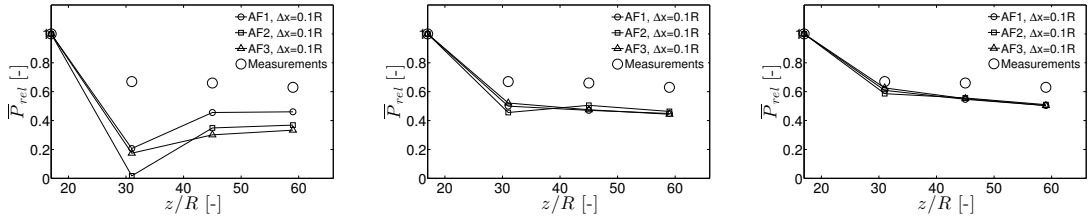

Figure 5. Relative mean power for TI_{amb}=0% (left), TI_{amb}=4.5% (middle) and TI_{amb}=8.9% (right) in the presence of wind turbines with a spacing of $14R$. TI_{amb} in the measurement case is always equal to 7%.

In Figure 4 it can be seen that there are significant deviations between the results from using the different rotor configurations when $TI_{amb} = 0\%$. For TI_{amb} =4.5% and 8.9% there are only small differences and, independent of the actual airfoil data and blade geometry, the computed results are generally in very good agreement with measurements. In all cases, it can be seen that for AF2, the second turbine in the row shows a slightly lower production compared to the production predicted by the other rotor configurations. When comparing the results when Δx is varied between $0.1R$ and $0.05R$ (right part of Figure 4), it can be seen that the production in general is marginally higher in the refined cases. However, when comparing the results from using the different rotor configurations, the differences are similarly small for $\Delta x = 0.1R$ as for $\Delta x = 0.05R$.

Figure 5 displays the same trends as Figure 4. The deviations between the rotors tend to become smaller when TI_{amb} increases. When TI_{amb}=4.5% and 8.9% the differences are seen to be limited. The general trend is that the production increases when TI_{amb} increases, regardless of airfoil and turbine spacing.

When comparing with the measurements, the agreement between the three rotor configurations is found to be good for the turbine spacing of $6.6R$ when TI_{amb} =4.5% and

8.9%. For $TI_{amb} = 0\%$ there are large differences for turbines 2 and 3 in the row for all rotor configurations. Further downstream the differences are however small. When the turbine spacing is $14R$ the simulations show larger deviations compared to the measured data than for a spacing of $6.6R$, but the general trends are the same as for a spacing of $6.6R$. The measurements are based on a filtering of the data using an inflow sector of 5° while the results from the computations are shown for flows that are fully aligned with the row of turbines. It is therefore expected that some underestimation of the power is experienced for the simulated cases. This underestimation should also be more pronounced for the $14R$ case since the distance between the turbines is larger. It is also noted that the turbines at Horns Rev have a nominal power of 2 MW and a rotor radius of 40 m while in the simulations a slightly larger rotor was used (as described in Section 2).

8.2. Relative mean thrust

The relative mean thrust ($\overline{T}_{rel}$) is in Figures 6 and 7 depicted as function of downstream distance for turbine spacings of $6.6R$ and $14R$, respectively. Similar trends as for $\overline{P}_{rel}$ are found as there are significant differences in $\overline{T}_{rel}$ when $TI_{amb} = 0\%$, regardless of turbine spacing. Furthermore, the differences in $\overline{T}_{rel}$ for the different rotor configurations are decreasing when TI_{amb} is increasing. Generally, when using imposed turbulence, AF3 predicts the highest value of $\overline{T}_{rel}$ while AF2 predicts the lowest. When comparing the results when Δx is varied between $0.1R$ and $0.05R$ (right part of Figure 6), it can be seen that the trends are again similar to those for $\overline{P}_{rel}$. Generally, $\overline{T}_{rel}$ is slightly higher for the refined case but the differences between the individual rotor configurations does not vary significantly between the different refinements.

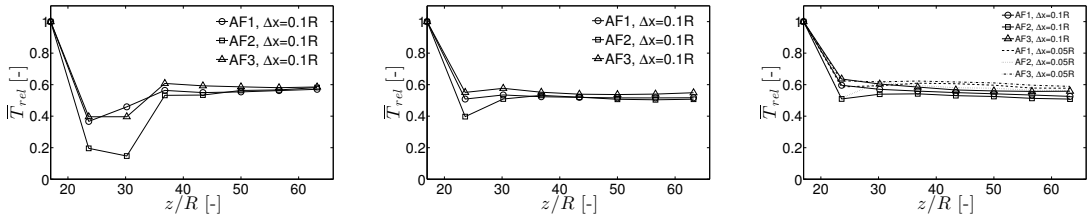

Figure 6. Relative mean thrust for TI_{amb}=0% (left), TI_{amb}=4.5% (middle) and TI_{amb}=8.9% (right) in the presence of wind turbines with a spacing of $6.6R$.

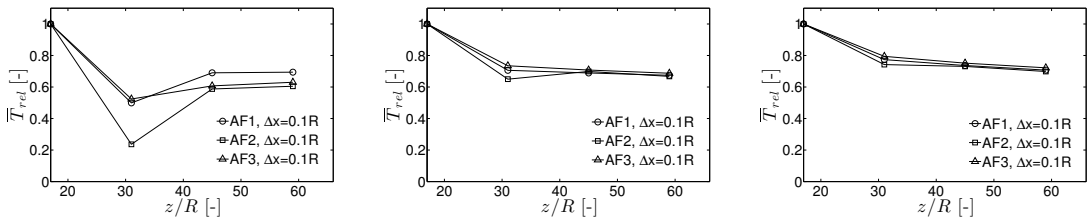

Figure 7. Relative mean thrust for TI_{amb}=0% (left), TI_{amb}=4.5% (middle) and TI_{amb}=8.9% (right) in the presence of wind turbines with a spacing of $14R$.

8.3. Normalized mean streamwise velocity

The normalized mean streamwise velocity ($\overline{W}_{norm}$) is in Figures 8 and 9 depicted as function of downstream distance for turbine spacings of $6.6R$ and $14R$, respectively.

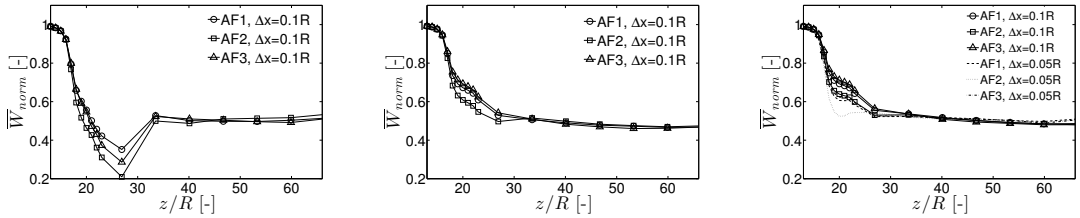

Figure 8. Normalized mean streamwise velocity for TI_{amb}=0% (left), TI_{amb}=4.5% (middle) and TI_{amb}=8.9% (right) in the presence of wind turbines with a spacing of $6.6R$.

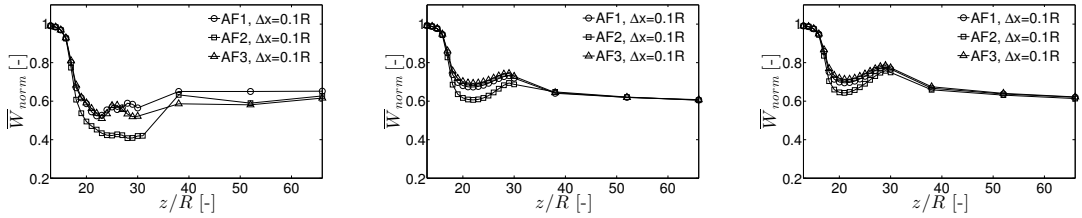

Figure 9. Normalized mean streamwise velocity for TI_{amb}=0% (left), TI_{amb}=4.5% (middle) and TI_{amb}=8.9% (right) in the presence of wind turbines with a spacing of $14R$.

In Figure 8 it can be seen that there are significant deviations between the computed results when $TI_{amb} = 0\%$ for z positions up to $z = 32R$. Further downstream the differences between the computed results of the different rotor configurations are small. For TI_{amb}=4.5% and 8.9% the velocities predicted using AF1 and AF3 are very similar. However, AF2 shows a lower velocity up until $z = 27R$. Further downstream this velocity is similar to those predicted using AF1 and AF3. When comparing the results when Δx is varied between $0.1R$ and $0.05R$ (right part of Figure 8), it can be seen that refined cases results in a lower mean velocity up until approximately $27R$ after which there are only very small differences between using the different resolutions. Additionally, using different resolution does not affect the differences between the rotor configurations.

In Figure 9 significant differences between the computed results are found up until $z = 31R$ for $TI_{amb} = 0\%$. In this case, in contrast to the results shown in Figure 8, the velocities do not merge after this distance as deviations are still found. These differences are however not as pronounced as those before $z = 31R$. For TI_{amb}=4.5% and 8.9% the same trends are found as in Figure 8, i.e., the velocities predicted using AF1 and AF3 are very similar and AF2 initially predicts a lower velocity, after which it later approaches the same velocity as obtained for the other rotor configurations.

8.4. Turbulence intensity

In Figures 10 and 11 the turbulence intensity (TI_{WT}) is shown as a function of the downstream distance for turbine spacings of $6.6R$ and $14R$, respectively.

In Figure 10 it can be seen that TI_{WT} shows a very similar behavior for AF1 and AF3 for all values of TI_{amb}. For $TI_{amb} = 0\%$, TI_{WT} when using AF2 shows a slightly different behavior which is especially evident for z distances up to $40R$. After this distance and for the other values of TI_{amb} all three rotor configurations show a similar behavior of TI_{WT}. When comparing the results when Δx is varied between $0.1R$ and $0.05R$ (right part of Figure 10), it can be seen that the refined simulations generally render slightly higher values of TI_{WT} compared to the coarser simulations. However, the differences between using the different rotor configurations does not

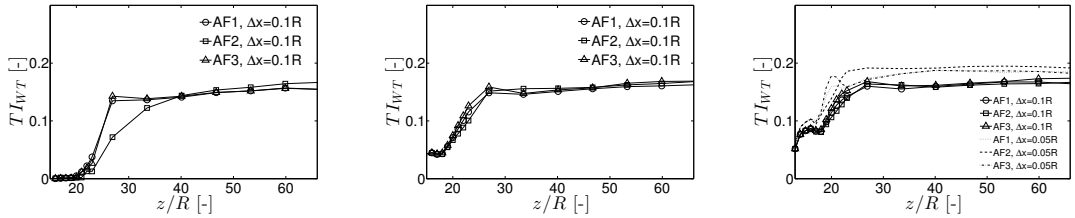

Figure 10. Turbulence intensity in the wake for TI_{amb}=0% (left), TI_{amb}=4.5% (middle) and TI_{amb}=8.9% (right) with presence of wind turbines with a spacing of 6.6R.

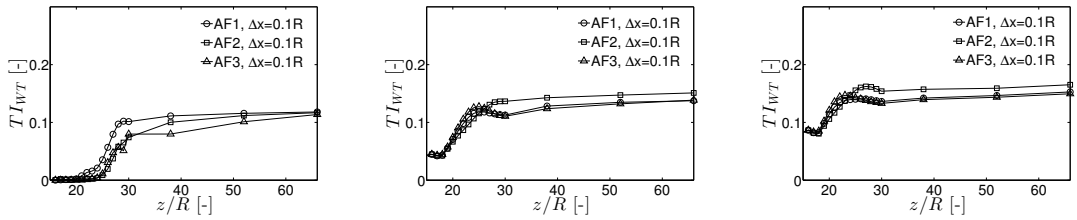

Figure 11. Turbulence intensity in the wake for TI_{amb}=0% (left), TI_{amb}=4.5% (middle) and TI_{amb}=8.9% (right) with presence of wind turbines with a spacing of 14R.

vary significantly when changing the resolution.

In Figure 11 there is a difference in the computed TI_{WT} when $TI_{amb} = 0\%$, but the values for the different rotor configurations are approaching each other at the last measurement point. For the other values of TI_{amb}, AF1 and AF3 show a very similar behavior for TI_{WT}. Using AF2, however, results in a TI_{WT} which is approximately 1% higher than for the two other cases. The general trend is that TI_{WT} is increasing with downstream distance. The slope of this increase is similar for all three rotor configurations.

9. Conclusions

LES simulations using an ACD method representing the rotor was performed using three different rotor configurations subject to different inflow conditions (level of ambient turbulence) and turbine spacing. The goal of the study was to analyze the mean wake flow characteristics, and the relative mean power production and thrust of the rotors in order to determine the importance of the choice of actual rotor geometry and airfoil data in ACD simulations. In the study, relative mean power and thrust were analyzed together with normalized mean streamwise velocity and turbulence intensity. It was found that the the choice of airfoil and rotor configuration became less important for higher levels of turbulence. For the low turbine spacing and a turbulent flow, none of the investigated parameters differed significantly from each other when comparing the computed results from the different rotor configurations. For the high turbine spacing only the computed turbulence intensity level differed between the different rotor configuration, whereas power production, thrust and mean streamwise velocity remained the same, provided that the inflow was turbulent. As a general conclusion it can be stated that the choice of airfoil data and actual rotor geometry in ACD simulations is not crucial if the intention of the simulations is to compute the mean wake characteristics subject to turbulent inflow.

10. Acknowledgments

The computations were performed on resources provided by the Swedish National Infrastructure for Computing (SNIC) at the National Supercomputer Centre (NSC). The present work has been

partly carried out with the support of the Danish Council for Strategic Research for the project 'Center for Computational Wind Turbine Aerodynamics and Atmospheric Turbulence' (grant 2104-09-067216/DSF) (COMWIND) (http://www.comwind.org).

References

[1] Sørensen JN and Myken A 1992 Unsteady Actuator Disc Model for Horizontal Axis Wind Turbines *Journal of Wind Engineering and Industrial Aerodynamics* **39** 139-149
[2] Nilsson K, Ivanell S, Hansen KS, Mikkelsen R, Breton S-P and Henningson D 2014 Large-eddy simulations of the Lillgrund wind farm *Wind Energy* DOI: 10.1002/we.1707
[3] Ivanell S, Mikkelsen R, Sørensen JN and Henningson D 2008 Three-dimensional actuator disc modeling of wind farm wake interaction *Proceeding of the European Wind Energy Conference and Exhibition 2008* Brussels, Belgium
[4] Porté-Agel F, Wu Y-T, Lu H and Conzemius RJ 2011 Large-eddy simulation of atmospheric boundary layer flow through wind turbines and wind farms *Journal of Wind Engineering and Industrial Aerodynamics* **99** 154-168
[5] Troldborg N, Sørensen JN and Mikkelsen R 2010 Numerical simulations of wake characteristics of a wind turbine in uniform inflow *Wind Energy* **13** 86-99
[6] Troldborg N, Larsen GC, Madsen HA, Hansen KS, Sørensen JN and Mikkelsen R 2011 Numerical simulations of wake interaction between two wind turbines at various inflow conditions *Wind Energy* **14** 859-876
[7] Churchfield MJ, Lee S, Michalakes J and Moriarty PJ 2012 A numerical study of the effects of atmospheric and wake turbulence on wind turbine dynamics *Journal of Turbulence* **13** N14 DOI: 10.1080/14685248.2012.668191
[8] Keck R-E, Mikkelsen R, Troldborg N, de Maré M and Hansen KS 2013 Synthetic atmospheric turbulence and wind shear in large eddy simulations of wind turbine wakes *Wind Energy* DOI: 10.1002/we.1631
[9] Troldborg N, Sørensen JN, Mikkelsen R and Sørensen NN 2014 A simple atmospheric boundary layer model applied to large eddy simulations of wind turbine wakes *Wind Energy* **17** 657-669
[10] Crespo A, Hernández J and Frandsen S 1999 Survey of Modelling Methods for Wind Turbine Wakes and Wind Farms *Wind Energy* **2** 1-24
[11] Vermeer LJ, Sørensen JN and Crespo A 2003 Wind turbine wake aerodynamics *Progress in Aerospace Sciences* **39** 467-510
[12] Jonkman J, Butterfield S, Musial W and Scott G 2009 Definition of a 5-MW Reference Wind Turbine for Offshore System Development *Technical report NREL/TP-500-38060* National Renewable Energy Laboratory
[13] Churchfield MJ 2013 Generic Siemens SWT-2.3-93 Specifications *WakeBench document* National Renewable Energy Laboratory
[14] Michelsen JA 1992 Basis3D - A Platform for Development of Multiblock PDE Solvers *Technical report AFM 92-05* Technical University of Denmark
[15] Michelsen JA 1994 Block Structured Multigrid Solution of 2D and 3D Elliptic PDE's *Technical report AFM 94-06* Technical University of Denmark
[16] Sørensen NN 1995 General purpose flow solver applied to flow over hills *PhD thesis Risø-R-827-(EN)* Risø National Laboratory
[17] Mikkelsen R 2003 Actuator Disc Methods Applied to Wind Turbines *PhD thesis MEK-FM-PHD 2003-02* Technical University of Denmark
[18] Ivanell S, Mikkelsen R, Sørensen JN and Henningson D 2008 Validation of methods using EllipSys3D *Technical report TRITA-MEK 2008:12* KTH Engineering Sciences
[19] Ta Phuoc L 1994 Modèles de sous maille appliqués aux écoulmements instationnaires décollés *Technical report LIMSI 93074* LIMSI France
[20] Mann J 1994 The spatial structure of neutral atmospheric surface-layer turbulence *Journal of Fluid Mechanics* **273** 141-168
[21] Mann J 1998 Wind field simulation *Probabilistic Engineering Mechanics* **13** 269-282
[22] Hansen KS 2011 Guidelines to wind farm analysis Upwind WP1A2 & WP8 Technical University of Denmark.
[23] Hansen KS, Barthelmie RJ, Jensen LE and Sommer A 2012 The impact of turbulence intensity and atmospheric stability on power deficits due to wind turbine wakes at Horns Rev wind farm *Wind Energy* **15** 183-196